# A Micromechanical Model for Textile Composite Plates

RAMESH V. MARREY* AND BHAVANI V. SANKAR**
*Center for Studies of Advanced Structural Composites*
*Department of Aerospace Engineering, Mechanics & Engineering Science*
*University of Florida*
*Gainesville, FL 32611-6250*

(Received January 11, 1996)
(Revised June 9, 1996)

**ABSTRACT:** A novel finite element based micromechanical method is developed for computing the plate stiffness coefficients ($A$, $B$, $D$ matrices) and coefficients of thermal expansion ($\alpha$'s and $\beta$'s) of a textile composite modeled as a homogeneous plate. Periodic boundary conditions for the plate model, which are different from those for the continuum model, have been derived. The micromechanics methods for computing the coefficients of thermal expansion are readily extended to compute the thermal residual stresses due to curing. The methods are first verified by applying to several examples for which solutions are known, and then applied to the case of woven composites. The plate stiffness coefficients computed from direct micromechanics are compared with those derived from the homogenized elastic constants in conjunction with the classical plate theory. It is found that the plate stiffness coefficients of textile composites, especially the $B$ and $D$ matrices, cannot be predicted from the homogenized elastic constants and the plate thickness.

**KEY WORDS:** fiber composites, finite elements, homogenization, micromechanics, textile composites, thermal stresses, unit-cell analysis, woven composites.

## 1. INTRODUCTION

CURRENTLY THE TWO well established methods of manufacturing fiber composite structural elements are filament winding and lamination of prepregs. Although filament winding is a highly automated process, it imposes limitations on the shape and curvature of the parts and also on the fiber orientations (Peters et al., 1990). The lamination method is labor intensive, which results in

*Postdoctoral Research Associate, currently with Advance USA, Old Lyme, CT.
**Professor and Director.



0021-9983/97/12 1187-27 $10.00/0

increased processing cost and time. Only plate or shell type structures can be fabricated using the lamination process, which limits the shape and size of the structures built. Further, laminated composites possess a weak interlaminar plane, where damage can initiate and cause delamination as in low-velocity foreign object impact. These factors have limited the use of fiber composites in a variety of structures.

Recent developments in textile technology and composite processing techniques seem to be promising in overcoming the aforementioned difficulties. Advances in textile technology have given rise to novel weaving and braiding techniques, which can be used to weave or braid fibers into structural preforms of complicated shapes. The skeletal preforms can be impregnated with appropriate matrix materials in molds to create composite structural components. The modern weaving and braiding machines can also produce structural shapes such as seamless cylinders, cones, domes and beams of various cross-sections such as I, H, L, etc. Textile composites do not have interlaminar planes as in tape laminates, although they have inter-yarn regions. However the impact resistance of textile composites, eg., braided composites (Gong and Sankar, 1991), seem to be higher than laminated composites due to the intertwining nature of the fiber tows. Further, the preforms can be stitched together using fiber materials, such as glass or Kevlar®, before resin impregnation to form integral parts, thus avoiding various types of joints (Dexter and Funk, 1986; Sharma and Sankar, 1995). Resin transfer molding—a faster and less labor intensive fabrication process—combined with the three-dimensional fiber preforms can greatly reduce the manufacturing time and cost of composite parts.

With the advancements in aforementioned technologies there is a need to develop scientific methods of predicting the mechanical behavior of textile composites. There are numerous variables involved in textile processes besides the choice of the fiber and matrix materials that will affect the properties of the composite. This, for example, includes the number of filaments in the yarn specified by the yarn linear density, and the fiber architecture determined by the type of weaving or braiding processes. Ideally, a structural engineer would like to model textile composites as a homogeneous anisotropic material—preferably orthotropic—so that the structural computations can be simplified, and also the existing computer codes can be used in the design. Thus, there is a need to predict the macroscopic properties of the composites from the micromechanical details such as fiber and matrix properties, fiber-matrix interface characteristics and the fiber architecture. This will be possible, if we assume that there is a representative volume element or a unit-cell that repeats itself throughout the volume of the composite, which seems to be true in the case of textile composites. Any variations that may occur near the free edge or a hole, and the inhomogeneities intrinsic to the manufacturing process have to be dealt separately as a perturbation in the homogeneous material.

An extensive amount of work on modeling textile composite materials has been done by Chou and his coworkers. Ishikawa and Chou (1982, 1983a, 1983b) developed the mosaic, fiber undulation and fiber bridging models to predict the thermo-mechanical behavior of woven composites. The basic principle in their

model is to approximate the woven composite as a composite laminate and compute the properties using lamination theory. Corrections are applied to account for the fiber continuity in the thickness direction and the fiber undulations that occur in the woven composite. Ma et al. (1986) developed an energy approach to determine the elastic constants of three-dimensional braided composites. Whitney and Chou (1989) extended the method to 3-D angle interlock composites. All these methods are simple to apply, but yield only approximate results. However, they will be very useful in the preliminary selection of textile process and in generating performance maps of composites for various fiber architectures (Yang and Chou, 1987).

A detailed micromechanical stress analysis of woven composites was performed by Yoshino and Ohtsuka (1982) using finite elements. They modeled the unit-cell of a plain-weave glass/epoxy using plane triangular elements to identify the regions of initiation of failure, which were verified using photoelastic experimental analysis. Dasgupta et al. (1990) used a homogenization scheme to predict the effective thermo-elastic properties of woven fabric composites. The microscale boundary value problem was solved using the finite element method. Whitcomb (1991) analyzed the unit-cell of a plain-weave composite using three-dimensional finite elements to determine the effect of the yarn geometry and yarn volume fraction on the composite thermo-elastic constants. He took advantage of some symmetry in the way yarns are stacked and avoided using explicit periodic boundary conditions. Foye (1993) developed a finite element scheme in which the unit-cell was modeled using inhomogeneous elements called replacement elements. The model was able to predict the elastic constants reasonably well. There are several other models that idealize the textile composite as simple structures and use lamination theory or strength of material approach to determine the elastic constants. Naik (1994) used a simple stiffness averaging method to compute the effective thermo-elastic constants of various textile composites. Sankar and Marrey (1993) studied the stress gradient effects in thin textile composite beams by performing a finite element analysis of the unit-cell. They computed the flexural rigidity and transverse shear stiffness of a plain-weave beam, and showed that the beam stiffness properties could not have been predicted from the equivalent elastic constants of the material and beam thickness.

This paper is concerned with a direct micromechanical approach for computing the plate thermo-mechanical properties of a textile composite plate. The unit-cell is analyzed using three-dimensional finite elements. In Section 2 the periodic boundary conditions for modeling the composite as a homogeneous material are described for the sake of completion. The modified approach for textile composite plates is described in Section 3. The methods for computing thermal residual stresses are given in Section 4. The results are discussed in Section 5. The methods are verified first by applying to some simple cases and comparing the results with available analytical solutions. Then, the current methods are applied to the case of a plain-weave composite plate and a five-harness satin-weave plate. It is shown that the plate stiffness and plate thermal expansion coefficients cannot be computed from the thermo-elastic constants obtained by using the conventional homogenization procedures.

## 2. MODELING TEXTILE COMPOSITES AS HOMOGENEOUS MATERIALS

In this section, we describe a finite element based micromechanical analysis procedure to predict the effective stiffness properties and coefficients of thermal expansion of a textile composite modeled as a homogeneous material (thermoelastic constants of the homogenized medium). The macroscopic properties of the composite are determined at a scale much larger than the dimensions of the unit-cell, but comparable to the dimensions of the structural component. The average stresses at a point at the structural scale will be called the macroscale stresses or macrostresses. The actual stresses at a point at the continuum level—either in the yarn or in the interstitial matrix—will be called the microscale stresses or microstresses. In order to distinguish the macroscale deformations and stresses from their microscale counterparts, a superscript "$M$" will be used to denote the macroscale quantities.

In the unit-cell analysis we assume that the textile composite is subjected to a uniform state of strain at the macroscale, and the average stresses (macrostresses) required to create such a state of strain are computed from the finite element model. In the microscale, the stresses within the unit-cell (microstresses) may not be uniform, but all unit-cells will have identical stress and strain fields. Thus the variation of stresses and strains will be periodic. Continuity of stresses across the unit-cell then requires that tractions be equal and opposite at corresponding points on opposite faces of the unit-cell. Since the displacement gradients are constant for a homogeneous deformation, the displacements at corresponding points on opposite faces of the unit-cell differ only by a constant (Sankar and Marrey, 1993). Consider a rectangular parallelepiped as the unit-cell of the three-dimensional textile composite as shown in Figure 1. The edges of the unit-cell are assumed to be parallel to the coordinate axes $x_1$, $x_2$ and $x_3$, with unit-cells repeating in all three directions. The length of the unit-cell in the $x_i$ direction is defined as $L_i$. On the macroscale the composite is assumed to be homogeneous, and its behavior characterized by the following constitutive relation:

$$\begin{Bmatrix} \sigma_{11}^M \\ \sigma_{22}^M \\ \sigma_{33}^M \\ \tau_{23}^M \\ \tau_{31}^M \\ \tau_{12}^M \end{Bmatrix} = \begin{bmatrix} C_{11} & C_{12} & C_{13} & C_{14} & C_{15} & C_{16} \\ & C_{22} & C_{23} & C_{24} & C_{25} & C_{26} \\ & & C_{33} & C_{34} & C_{35} & C_{36} \\ & \text{(symmetric)} & & C_{44} & C_{45} & C_{46} \\ & & & & C_{55} & C_{56} \\ & & & & & C_{66} \end{bmatrix} \left\{ \begin{Bmatrix} \epsilon_{11}^M \\ \epsilon_{22}^M \\ \epsilon_{33}^M \\ \gamma_{23}^M \\ \gamma_{31}^M \\ \gamma_{12}^M \end{Bmatrix} - \begin{Bmatrix} \alpha_1^c \\ \alpha_2^c \\ \alpha_3^c \\ \alpha_{23}^c \\ \alpha_{31}^c \\ \alpha_{12}^c \end{Bmatrix} \Delta T \right\} \quad (1)$$

where $\{\sigma^M\}$ and $\{\epsilon^M\}$ are the macroscale stresses and strains, respectively; $\{\alpha^c\}$ and $[C]$ are respectively the macroscale CTE's and elasticity matrix to be determined; and $\Delta T$ is a uniform temperature difference throughout the unit-cell†. The temperature difference $\Delta T$ is computed from a reference state at which no

†There are situations wherein the microscale temperature will vary within the unit-cell, e.g., the heat transfer problem to determine the effective thermal conductivities of a textile composite (Hart, 1994).

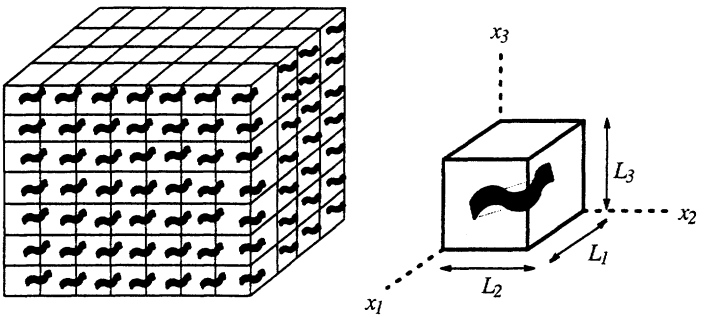


***Figure 1.*** *Unit-cell of a three-dimensional textile composite.*

stresses exist. For the purpose of determining the residual thermal stresses due to fabrication, the temperature difference is measured from the composite curing temperature.

The periodic boundary conditions (BC's) consist of: (a) periodic displacement boundary conditions, which ensure compatibility of displacements on the opposite faces of the unit-cell; and (b) periodic traction boundary conditions to enforce the continuity of stresses across the unit-cell boundaries. A macroscopically homogeneous deformation can be represented as

$$u_i^M = H_{ij} x_j \quad i,j = 1,2,3 \tag{2}$$

where $H_{ij}$ are the displacement gradients. Then the periodic displacement boundary conditions to be imposed between nodes on the faces $x_i = 0$ and $x_i = L_i$ are:

$$\begin{aligned} u_i(L_1,x_2,x_3) - u_i(0,x_2,x_3) &= H_{i1}L_1 \\ u_i(x_1,L_2,x_3) - u_i(x_1,0,x_3) &= H_{i2}L_2 \\ u_i(x_1,x_2,L_3) - u_i(x_1,x_2,0) &= H_{i3}L_3 \end{aligned} \tag{3}$$

The traction boundary conditions to be imposed on the faces $x_i = 0$ and $x_i = L_i$ are:

$$\begin{aligned} F_i(L_1,x_2,x_3) &= -F_i(0,x_2,x_3) \\ F_i(x_1,L_2,x_3) &= -F_i(x_1,0,x_3) \\ F_i(x_1,x_2,L_3) &= -F_i(x_1,x_2,0) \end{aligned} \tag{4}$$

In Equations (3) and (4) the index $i$ takes values 1 through 3. The above periodic

BC's are imposed in the finite element model by using multi-point constraint elements or by using transformation equations to eliminate the constrained displacements (Cook et al., 1989). Both methods require a finite element model in which opposite faces of the unit-cell have identical FE mesh so that periodic BC's can be imposed between corresponding nodes. The periodic BC's are summarized in the first six rows in Table 1.

The unit-cell is discretized with three-dimensional finite elements, e.g., eight-node brick elements, such that opposite faces of the unit-cell have identical nodes. Periodic displacement and traction boundary conditions are enforced as explained above. The periodic displacement BC's are imposed such that only one of the components of the macrostrains is non-zero, and the uniform temperature difference $\Delta T$ is set to zero. Then the difference in displacements between corresponding points on opposite faces of the unit-cell will be equal to that in a homogenous material subject to the same deformation. The average stresses (macrostresses) required to create such a deformation are obtained from the finite element results. Two different methods of computing macrostresses are presented at the end of this section. Substituting the macrostresses and macrostrains in the composite constitutive relation given by Equation (1), the stiffness coefficients in the column corresponding to the non-zero macrostrain can be evaluated. For example, if we assume that $\epsilon_{11}^M = 1$ and all other macrostrains to be equal to zero (Case 1 in Table 1), then from the macrostresses we should be able to compute the first column $C_{i1}$ of $[C]$. This procedure is repeated for other macrostrain components (keeping the temperature difference as zero) to obtain the entire stiffness matrix $[C]$. The elastic constants of the composite material can be easily determined by inverting the stiffness matrix to obtain the compliance matrix $[S]$, and comparing the compliance coefficients with that of an anisotropic material, e.g., $S_{11} = 1/E_1$, (Agarwal and Broutman, 1990). It can be shown that the stiffness

***Table 1. Periodic displacement BC's to obtain 3-D elastic constants and CTE's.***

| | Macrostrain | Non-Zero Displacement BC's |
|---|---|---|
| 1. | $\epsilon_{11}^M = 1$ | $u_1(L_1, x_2, x_3) - u_1(0, x_2, x_3) = L_1$ |
| 2. | $\epsilon_{22}^M = 1$ | $u_2(x_1, L_2, x_3) - u_2(x_1, 0, x_3) = L_2$ |
| 3. | $\epsilon_{33}^M = 1$ | $u_3(x_1, x_2, L_3) - u_3(x_1, x_2, 0) = L_3$ |
| 4. | $\gamma_{23}^M = 1$ | $u_2(x_1, x_2, L_3) - u_2(x_1, x_2, 0) = L_3/2$<br>$u_3(x_1, L_2, x_3) - u_3(x_1, 0, x_3) = L_2/2$ |
| 5. | $\gamma_{31}^M = 1$ | $u/(x_1, x_2, L_3) - u_1(x_1, x_2, 0) = L_3/2$<br>$u_3(L_1, x_2, x_3) - u_3(0, x_2, x_3) = L_1/2$ |
| 6. | $\gamma_{12}^M = 1$ | $u_1(x_1, L_2, x_3) - u_1(x_1, 0, x_3) = L_2/2$<br>$u_2(L_1, x_2, x_3) - u_2(0, x_2, x_3) = L_1/2$ |
| 7. | $\Delta T = T_0$ | All relative displacements are set to zero |
| | All macrostrains set to zero | |

matrix $[C]$ computed by using the procedure described above will always be symmetric (see Appendix).

To compute the six CTE's, a finite temperature change $\Delta T$, is applied to all elements in the unit-cell, and periodic displacement BC's are imposed such that all the macrostrain components are zero. Then the composite constitutive relation (Equation 1) will reduce to

$$\{\sigma^M\} = -[C]\{\alpha^c\}\Delta T \tag{5}$$

The macrostresses for such a deformation are computed by using one of the two procedures described at the end of this section. Since the stiffness matrix $[C]$ is known, the composite CTE's can be found from Equation (5) as:

$$\{\alpha^c\} = -\frac{1}{\Delta T}[C]^{-1}\{\sigma^M\} \tag{6}$$

The last row in Table 1 presents the periodic displacement BC's imposed on the unit-cell to obtain the CTE's $\{\alpha^c\}$. It may be noted that the value of $\Delta T$ is arbitrary and usually taken as unity.

The macrostresses for a given deformation state can be found by one of the following two methods. In the first method, the macrostresses are obtained by averaging the nodal forces on each face of the unit cell. For example, the macrostress component $\sigma_{11}^M$ can be obtained as

$$\sigma_{11}^M = \frac{1}{L_2L_3}\sum_n F_1^{\{n\}}(L_1,x_2,x_3) \tag{7}$$

where $F_1^{\{n\}}$ is the nodal force in the $x_1$ direction at the $n$th node, and $\Sigma_n$ denotes summation over all nodes on the face $x_1 = L_1$. Alternatively, the macrostresses can be computed by volume-averaging the corresponding microstress component in the unit-cell. Then $\sigma_{11}^M$ is obtained as

$$\sigma_{11}^M = \frac{1}{V}\int_V \sigma_{11}(x,y,z)\,dV \tag{8}$$

where $V$ is the volume of the unit-cell. In the FE model Equation (8) is implemented by computing microstresses at the Gauss quadrature points, and by performing numerical integration over the volume in each element of the unit-cell. Even though expressions given by Equations (7) and (8) are equivalent, from the programming point of view Equation (8) is much easier to implement.

## 3. MODELING TEXTILE COMPOSITES AS HOMOGENEOUS PLATES

For efficient structural design, one may expect to use textile composites as thin-walled structures, e.g., plate/shell/beam. Unlike the model described in Section 2, thin-walled structures will have fewer unit-cells in the thickness direction, say

$z$-direction. This will violate the assumption of unit-cells repeating themselves in the $z$-direction. Further, the surfaces normal to the $z$-axis will be free of tractions, and there will be stress gradients through the thickness of the structure. In general, the textile composite will behave more like a plate than a three-dimensional structure. In that case the elastic constants computed in Section 2 will not be useful (Sankar and Marrey, 1993). In such situations it may be a good idea to use the homogenization procedure to compute the effective plate properties rather than the elastic constants. Thus one may need to compute plate stiffness coefficients, such as flexural stiffness. Typically composite plate theories use the so called $[A, B, D]$ matrices (Agarwal and Broutman, 1990). These stiffness coefficients cannot be calculated from the homogenized elastic constants computed using methods in Section 2. For example, if one uses the macroscale elastic constants computed from $[C]$, then one will be computing the plate stiffness using formulas of the type‡ $D = Eh^3/12(1 - \nu^2)$, which is not the true representation of the textile composite plate behavior. In some situations the elastic constants of the homogenized material will not reflect the bending-stretching coupling that may really exist in the textile composite plate. This coupling will reveal itself by a non-zero $[B]$ in the plate model.

In the following we suggest a micromechanical analysis for modeling textile composites as homogeneous plates, and describe a procedure to compute the $[A]$, $[B]$ and $[D]$ matrices directly from the micromechanics rather than computing them from the elastic constants of the homogenized continuum and the plate thickness. The procedure is analogous to that for estimating the continuum properties (Section 2) except for the periodic boundary conditions. The major difference is that the top and bottom surfaces of the plate—planes normal to the $z$-axis—are left traction-free, i.e., no constraints are imposed between the nodes on the top and bottom surfaces [Figure 2(a)]. Periodic boundary conditions are applied only between nodes on the two pairs of lateral surfaces as explained later. The textile composite plate is assumed to be in the $xy$-plane with unit-cells repeating in the $x$- and $y$- directions. The mid-plane of the plate is assumed to coincide with the $y$-plane. The lengths of the unit-cell in the $x$- and $y$-directions are assumed to be $a$ and $b$ respectively, and the unit-cell thickness as $h$. On the macroscale the plate is assumed to be homogeneous and the plate behavior is characterized by the Classical Plate Theory constitutive relations:

$$\begin{bmatrix} A_{11} & A_{12} & A_{16} & B_{11} & B_{12} & B_{16} \\ A_{22} & A_{22} & A_{26} & B_{12} & B_{22} & B_{26} \\ A_{16} & A_{26} & A_{66} & B_{16} & B_{26} & B_{66} \\ B_{11} & B_{12} & B_{16} & D_{11} & D_{12} & D_{16} \\ B_{12} & B_{22} & B_{26} & D_{12} & D_{22} & D_{26} \\ B_{16} & B_{26} & B_{66} & D_{16} & D_{26} & D_{66} \end{bmatrix} \left\{ \begin{pmatrix} \epsilon_{x0}^M \\ \epsilon_{y0}^M \\ \gamma_{xy0}^M \\ \kappa_x^M \\ \kappa_y^M \\ \kappa_{xy}^M \end{pmatrix} - \begin{pmatrix} \alpha_x^p \\ \alpha_y^p \\ \alpha_{xy}^p \\ \beta_x^p \\ \beta_y^p \\ \beta_{xy}^p \end{pmatrix} \Delta T \right\} = \begin{pmatrix} N_x \\ N_y \\ N_{xy} \\ M_x \\ M_y \\ M_{xy} \end{pmatrix} \quad (9)$$

‡This is the formula for flexural rigidity of isotropic plates. $E$, $\nu$, and $h$ are the Young's modulus, Poisson's ratio and thickness of the plate, respectively.

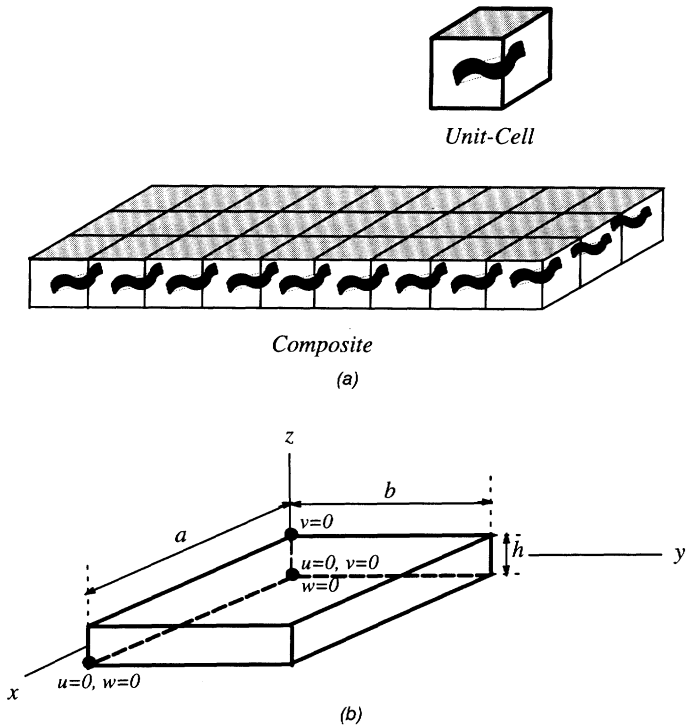


***Figure 2.*** *(a) Unit-cell of a textile composite plate and (b) support boundary conditions on the unit-cell.*

where $\epsilon_{i0}^M$, $\gamma_{i0}^M$ and $k_i^M$ are the midplane axial strain, midplane shear strain and curvatures, respectively; $\alpha_i^p$ and $\beta_i^p$ are the plate thermal expansion and bending coefficients; $N_i$ and $M_i$ are the axial force and bending moment resultants respectively in the homogeneous plate. The midplane strains and curvatures are related to the midplane displacements as:

$$\epsilon_{x0}^M = \frac{\partial u_0}{\partial x}, \quad \epsilon_{y0}^M = \frac{\partial v_0}{\partial y}, \quad \gamma_{xy0}^M = \frac{\partial u_0}{\partial y} + \frac{\partial v_0}{\partial x} \tag{10}$$

$$\varkappa_x^M = -\frac{\partial^2 w}{\partial x^2}, \quad \varkappa_y^M = -\frac{\partial^2 w}{\partial y^2}, \quad \varkappa_{xy}^M = -2\frac{\partial^2 w}{\partial x \partial y} \tag{11}$$

The plate thermo-mechanical properties are obtained by modeling the unit-cell with three-dimensional finite elements, e.g., eight-node brick elements, and subjecting the unit-cell to six linearly independent deformations (Table 2). The unit-cell is subjected to minimum support constraints to prevent rigid body rotation

and translation [Figure 2(b)]. The top and bottom surfaces of the plate were assumed to be free of tractions. The faces $x = 0$ and $x = a$ have identical nodes in the finite element model, and so do the pair of faces $y = 0$ and $y = b$. The corresponding nodes on opposite faces of the unit cell are constrained to enforce the periodic BC's. The traction boundary conditions on the lateral faces of the unit-cell were:

$$F_i(a,y,z) = -F_i(0,y,z), \quad F_i(x,b,z) = -F_i(x,0,z), \quad i = x,y,z \tag{12}$$

The periodic displacement boundary conditions are inferred as follows. Let us first consider the case where the plate is deformed in such a way that $\epsilon^M_{x0}$ is the only nonzero deformation. If the plate were homogeneous, then the relationship between displacements of corresponding nodes on the faces $x = 0$ and $x = a$ will be such that

$$u(a,y,z) - u(0,y,z) = a\epsilon^M_{x0} \tag{13}$$

The $v$ and $w$ components of relative displacements between points on planes $x = 0$ and $x = a$, and also all relative displacements between corresponding points on planes $y = 0$ and $y = b$ will be identically equal to zero. In the case of textile composite plates, the plate is assumed to behave as a homogeneous plate in macroscale, and hence the BC's in Equation (13) can be assumed to be valid

***Table 2. Periodic displacement BC's imposed on the lateral faces of the plate unit-cell.***

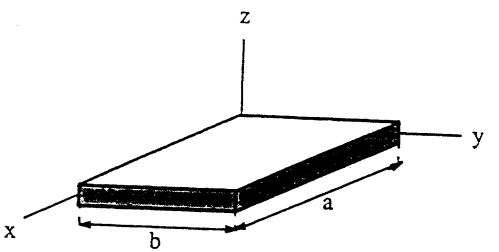


| | | $u(a,y)-u(0,y)$ | $v(a,y)-v(0,y)$ | $w(a,y)-w(0,y)$ | $u(x,b)-u(x,0)$ | $v(x,b)-v(x,0)$ | $w(x,b)-w(x,0)$ | $\Delta T$ |
|---|---|---|---|---|---|---|---|---|
| 1. | $\epsilon^M_{x0} = 1$ | $a$ | 0 | 0 | 0 | 0 | 0 | 0 |
| 2. | $\epsilon^M_{y0} = 1$ | 0 | 0 | 0 | 0 | $b$ | 0 | 0 |
| 3. | $\gamma^M_{xy0} = 1$ | 0 | $a/2$ | 0 | $b/2$ | 0 | 0 | 0 |
| 4. | $\kappa^M_x = 1$ | $az$ | 0 | $-a^2/2$ | 0 | 0 | 0 | 0 |
| 5. | $\kappa^M_y = 1$ | 0 | 0 | 0 | 0 | $bz$ | $-b^2/2$ | 0 |
| 6. | $\kappa^M_{xy} = 1$ | 0 | $az/2$ | $-ay/2$ | $bz/2$ | 0 | $-bx/2$ | 0 |
| 7. | $\Delta T = T_0$ | 0 | 0 | 0 | 0 | 0 | 0 | $T_0$ |

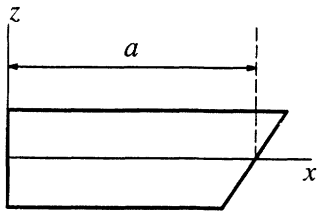


$$u(a,y,z) - u(0,y,z) = \varkappa_x^M az$$

(a)

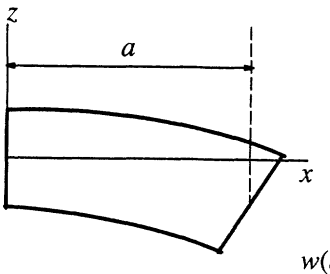


$$u(a,y,z) - u(0,y,z) = \varkappa_x^M az$$

$$w(a,y,z) - w(0,y,z) = -\varkappa_x^M \frac{a^2}{2}$$

(b)

***Figure 3.*** *Periodic displacement BC's for non-zero curvature.*

also. Similar BC's corresponding to $\epsilon_{y0}^M$ and $\gamma_{xy0}^M$ can be derived. They are presented in the first three rows of Table 2. These three boundary conditions are similar to the three boundary conditions for modeling the textile composite as a homogeneous material as explained in Section 2 (cf. rows, 1, 2, and 6 in Table 1).

The BC's for curvatures are derived as follows. Consider a plate that is deformed such that $\varkappa_x^M$ is the only nonzero deformation. Then the unit-cell will undergo cylindrical bending and will be bent in the shape of an arc of a circle with curvature equal to $\varkappa_x^M$ (see Figure 3). The plane $x = a$ will be rotated through an angle equal to $a\varkappa_x^M$ relative to the plane $x = 0$. Then the relative displacements between points on the pair of surfaces normal to the $x$-axis will be given by

$$u(a,y,z) - u(0,y,z) = \varkappa_x^M az \tag{14}$$

The displacement field defined by Equation (14) introduces a transverse shear deformation in the plate due to the presence of nonzero $\partial u/\partial z$. The effect of the boundary condition given by Equation (14) is depicted in Figure 3(a). This shear has to be eliminated by superposing transverse displacements given by

$$w(a,y,z) - w(0,y,z) = -\varkappa_x^M \frac{a^2}{2} \tag{15}$$

In deriving Equation (15), the circular arc mentioned above has been approx-

imated as a parabola. The effect of adding this transverse displacement is shown in Figure 3(b). Thus Equations (14) and (15) constitute the periodic displacement BC for the case of non-zero $\varkappa_x^M$. Similar BC's can be derived for cases where the nonzero deformations are $\varkappa_y^M$ and $\varkappa_{xy}^M$, respectively (Marrey, 1995; Sankar and Marrey, 1995). The periodic displacement BC's corresponding to the curvatures are presented in rows 4 through 6 of Table 2.

The macroscale force and moment resultants can be computed by averaging the actual force and moment resultant over the area of the plate unit-cell. Thus

$$(N_x, N_y, N_{xy}) = \frac{1}{ab} \int_A \left( \int_z (\sigma_{xx}, \sigma_{yy}, \tau_{xy}) dz \right) dA \tag{16}$$

In the above equation the inside integral represents the force resultant at a point in the plate unit-cell, and the outside integral represents averaging of the *micro-force-resultants* over the area of the plate to obtain *macro-force-resultants*. The above equation can be written as a volume integral over the volume of the unit-cell:

$$(N_x, N_y, N_{xy}) = \frac{1}{ab} \int_V (\sigma_{xx}, \sigma_{yy}, \tau_{xy}) dV \tag{17}$$

Similarly the macroscale moment resultants can be derived as

$$(M_x, M_y, M_{xy}) = \frac{1}{ab} \int_V z(\sigma_{xx}, \sigma_{yy}, \tau_{xy}) dV \tag{18}$$

In the FE model, integrations in Equations (17) and (18) were performed using the Gauss quadrature method.

The analysis procedures described above was carried out separately for six different cases. In each case, one of the six plate deformations was kept equal to unity, and the rest were set to zero. The macroscale force and moment resultants were computed for each case. The temperature difference was also set to zero in all six cases. Substituting the values of the deformation and the force resultants in the plate constitutive relation, Equation (9), the stiffness coefficients in the column corresponding to the non-zero deformation can be computed. Using a procedure similar to that described in the Appendix, it can be shown that the $[A, B, D]$ matrix must be symmetric.

To predict the CTE's, the plate unit cell is subjected to a uniform temperature difference, say $\Delta T = T_0$, and periodic displacement BC's are applied such that all six components of the macroscale deformations are zero (seventh case in Table 2). The force resultants $\{N\}$ and moment resultants $\{M\}$ are computed using the procedure described earlier. Then the plate constitutive relations (Equation 9) can be used to compute the unknown CTE's. The plate thermal expansion coefficients $\alpha^p$ and thermal bending coefficients $\beta^p$ are then obtained from the relation:

$$\begin{Bmatrix} \alpha^p \\ \beta^p \end{Bmatrix} = -\frac{1}{T_0} \begin{bmatrix} A & B \\ B & D \end{bmatrix}^{-1} \begin{Bmatrix} N \\ M \end{Bmatrix} \tag{19}$$

## 4. THERMAL RESIDUAL STRESSES

We will explain the procedure for computing thermal residual stresses in detail for the case of continuum modeling of the textile composite. Let $T_0$ be the difference between the composite fabrication temperature and the room temperature. Since the composite is assumed to be stress free at the fabrication temperature—which is above the room temperature, $\Delta T$ is generally negative, say $\Delta T = -T_0$. The residual microstresses in the yarn and the matrix are obtained by superposing the microstresses due to the two load cases as explained below. In the first load case [Figure 4(a)], the unit-cell is constrained from expanding by fixing the eight corner nodes of the unit-cell and enforcing zero displacement difference and equal-opposite tractions between corresponding nodes on opposite faces of the unit-cell (periodic BC's). A temperature difference $\Delta T$ is applied to all elements in the finite element model. This is exactly the same problem we solve for finding the three-dimensional CTE's. The applied boundary conditions mean that all the macroscopic strain components are equal to zero ($\{\epsilon^M\} = 0$, $\Delta T = -T_0$). Then the corresponding macroscopic stresses required to restrain the unit-cell expansion can be derived from Equation (1) as:

$$\{\sigma^M\} = [C]\{\alpha^c\}T_0 \tag{20}$$

In the second load case [Figure 4(b)], deformations are applied to the unit-cell so as to reverse the macrostresses developed in the first load case. This is because a cured composite plate is not subjected to any net external forces, and hence the macrostresses must be zero. This can be accomplished by imposing a set of deformations given by $\{\epsilon^M\} = -\{\alpha^c\}T_0$ on the unit-cell and setting $\Delta T = 0$. It may be noted that the macrostresses due to the deformations in the second loading case are equal to $-[C]\{\alpha^c\}T_0$, which are equal and opposite to the macrostresses given in Equation (20). The microstresses from both load cases are superposed to obtain the residual microstresses due to free thermal expansion.

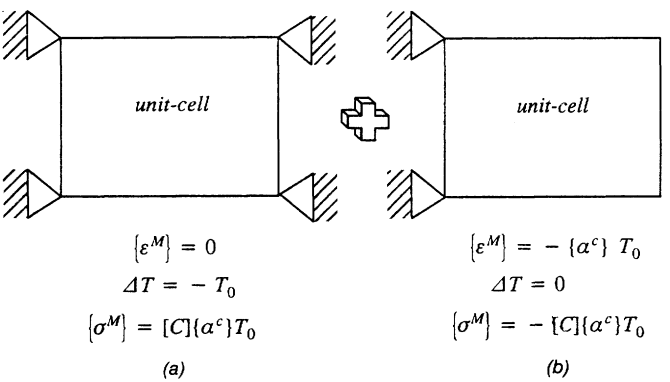


***Figure 4.*** *Load cases to compute the thermal residual microstresses.*

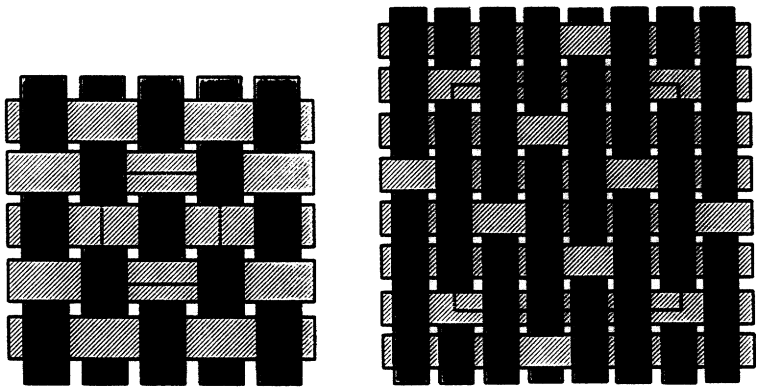


***Figure 5.*** *Yarn pattern in textile preforms (unit-cell boundary in dotted lines): (a) plain-weave and (b) 5-harness satin-weave.*

The same idea can be extended to finding the residual microstresses in the plate model also. Then, the deformations to be applied to the unit-cell in the first load case are: $\{\epsilon^M\} = 0$, $\{\varkappa^M\} = 0$ and $\Delta T = -T_0$; and the deformations in the second load case are: $\{\epsilon^M\} = -\{\alpha^P\}T_0$, $\{\varkappa^M\} = -\{\beta^P\}T_0$ and $\Delta T = 0$.

## 5. RESULTS AND DISCUSSION

The micromechanics procedures described in Sections 2 through 4 were first verified by applying them to problems for which exact solutions are known. Then they were applied to the case of unidirectional fiber composites for which approximate analytical solutions are available. Finally, several textile architectures were considered and compared with available experimental and analytical solutions. The examples considered can be classified as follows: Ex. 1. Bimaterial medium—both materials are assumed isotropic; Ex. 2. Unidirectional composite with different Poisson's ratios for fiber and matrix, fiber and matrix materials are isotropic; Ex. 3. Plain-weave textile composite (yarn geometry and properties obtained from Dasgupta et al., 1990); Ex. 4. Plain-weave textile composite (yarn geometry and properties obtained from Naik, 1994); Ex. 5. Five-harness satin weave (yarn geometry and properties obtained from Naik, 1994). In the textile composite examples, Examples 3–5 [Figures 5(a) and 5(b)], the yarn is assumed to be transversely isotropic and the matrix material is assumed isotropic. The constituent material properties used in the examples are listed in Table 3.

The unit-cell was modeled using eight-node brick elements. We used the inhomogeneous elements similar to that developed by Foye (1993). The unit-cell was discretized using rectangular parallelepiped elements of uniform size. Thus there is a possibility that a given element would contain both yarn and matrix materials. The effect of the inhomogeneity within the element was accounted by considering appropriate elastic constants in the Gauss integration of the stiffness

matrix. For the plain weave composite the yarn shape was generated by translating an elliptical cross section along a sinusoidal path. The unit-cell was modeled using 15 × 15 × 10 mesh resulting in about 6,000 degrees of freedom. The problem was solved using a finite element program called $\mu$TE$\chi$ − 10, which was specially developed for NASA (Marrey and Sankar, 1995). This program has a built-in capability of enforcing periodic boundary conditions for both the continuum and plate models.

The results for continuum modeling of unit-cells in Examples 1–5 are given in Tables 4–6. The results for the bimaterial medium is given in Table 4. The bimaterial medium is an infinite solid with two alternating layers of isotropic materials. It may be noted that the present micromechanical model yields exact solution for all thermoelastic constants. This example is indeed a verification of the finite element program. The exact solution for the bimaterial medium was obtained by "rule of mixtures" type formulas, the details of which can be found in Marrey (1995) and Marrey and Sankar (1996). The thermoelastic constants of the unidirectional composite (Example 2) are compared with available analytical solutions in Table 5. The fibers were assumed to be of circular cross section in a square array. Rule of mixtures and Halpin-Tsai equations for elastic constants, and Schapery's expressions for CTE's were used to verify the present micromechanical results (Agarwal and Broutman, 1990). From Table 5 it may be seen that the agreement is good for all elastic constants except for $\nu_{TT}$ and also

***Table 3. Properties of constituent materials for Examples 1–5.***

| | |
|---|---|
| Example 1 | Layer 1 (E-glass): $E_1$ = 70 GPa, $\nu_1$ = 0.200, $\alpha_1$ = 5 × $10^{-6}$/°C, $V_1$ = 0.5<br>Layer 2 (epoxy): $E_2$ = 3.50 GPa, $\nu_2$ = 0.350, $\alpha_2$ = 60 × $10^{-6}$/°C, $V_2$ = 0.5<br>Unit-cell size: 0.500 × 0.500 × 0.256 mm |
| Example 2 | Fiber (E-glass): $E_f$ = 70 GPa, $\nu_f$ = 0.200, $\alpha_f$ = 5 × $10^{-6}$/°C, $V_f$ = 0.6<br>Matrix (epoxy): $E_m$ = 3.50 GPa, $\nu_m$ = 0.350, $\alpha_m$ = 60 × $10^{-6}$/°C<br>Unit-cell size: 10 × 10 × 10 $\mu$m |
| Example 3 | Yarn (glass-epoxy):<br>$E_L$ = 58.61 GPa, $E_T$ = 14.49 GPa, $G_{LT}$ = 5.38 GPa, $\nu_{LT}$ = 0.250<br>$\nu_{TT}$ = 0.247, $\alpha_L$ = 6.15 × $10^{-6}$/°C, $\alpha_T$ = 22.64 × $10^{-6}$/°C, $V_f$ = 0.26<br>Matrix (epoxy):<br>$E$ = 3.45 GPa, $\nu$ = 0.37, $\alpha$ = 69 × $10^{-6}$/°C<br>Unit-cell size: 1.680 × 1.680 × 0.228 mm |
| Examples 4,5 | Yarn (graphite-epoxy):<br>$E_L$ = 144.80 GPa, $E_T$ = 11.73 GPa, $G_{LT}$ = 5.52 GPa, $\nu_{LT}$ = 0.230<br>$\nu_{TT}$ = 0.300, $\alpha_L$ = −0.324 × $10^{-6}$/°C, $\alpha_T$ = 14.00 × $10^{-6}$/°C,<br>$V_f$ = 0.64 Matrix (epoxy):<br>$E$ = 3.45 GPa, $\nu$ = 0.35, $\alpha$ = 40 × $10^{-6}$/°C<br>Unit-cell size: 2.822 × 2.822 × 0.2557 mm (Example 4)<br>7.055 × 7.055 × 0.2557 mm (Example 5) |

$V_f$ stands for the volume fraction of the constituent material.

*Table 4. Continuum properties for bimaterial medium.*

| | | $E_x$, $E_y$ (GPa) | $E_z$ (GPa) | $G_{xy}$, $G_{yx}$ (GPa) | $G_{xy}$ (GPa) | $\nu_{xz}$, $\nu_{yz}$ | $\nu_{xy}$ | $\alpha_x^c$, $\alpha_y^c$ $\times 10^{-6}$/°C | $\alpha_z^c$ $\times 10^{-6}$/°C |
|---|---|---|---|---|---|---|---|---|---|
| Example 1 (bimaterial medium) | Present analysis | 36.79 | 9.79 | 2.48 | 15.23 | 0.312 | 0.208 | 8.19 | 59.60 |
| | Exact solution | 36.79 | 9.79 | 2.48 | 15.23 | 0.312 | 0.208 | 8.19 | 59.60 |

**Table 5. Continuum properties for unidirectional composite example.**

| | | $E_L$ (GPa) | $E_T$ (GPa) | $G_{LT}$ (GPa) | $G_{TT}$ (GPa) | $\nu_{LT}$ | $\nu_{TT}$ | $\alpha_L$ × $10^{-6}$/°C | $\alpha_T$ × $10^{-6}$/°C |
|---|---|---|---|---|---|---|---|---|---|
| Example 2 (unidirectional composite) | Present analysis | 43.12 | 18.15 | 5.59 | 3.92 | 0.242 | 0.222 | 7.40 | 25.44 |
| | Rule of mixt./ Halpin-Tsai equations | 43.40 | 14.79 | 4.45 | 5.91 | 0.260 | 0.252 | 6.77 | 34.24 |

*Table 6. Continuum properties for textile composite examples.*

| | | $E_x$, $E_y$ (GPa) | $E_z$ (GPa) | $G_{xy}$, $G_{yx}$ (GPa) | $G_{xy}$ (GPa) | $\nu_{xz}$, $\nu_{yz}$ | $\nu_{xy}$ | $\alpha_x^c$, $\alpha_y^c$ × $10^{-6}$/°C | $\alpha_z^c$ × $10^{-6}$/°C |
|---|---|---|---|---|---|---|---|---|---|
| Example 3 (Plain-weave) | Present analysis | 11.81 | 6.14 | 1.84 | 2.15 | 0.408 | 0.181 | 28.36 | 79.57 |
| | Dasgupta (1990) | 14.38 | 6.25 | 1.94 | 3.94 | 0.463 | 0.167 | 22.50 | 86.00 |
| Example 4 (Plain-weave) | Present analysis | 53.61 | 10.88 | 4.41 | 4.72 | 0.365 | 0.128 | 1.56 | 22.71 |
| | Naik (1994) | 64.38 | 11.49 | 5.64 | 4.87 | 0.396 | 0.027 | 1.33 | 20.71 |
| | Test (Foye, 1992) | 61.92 | — | — | — | — | 0.110 | — | — |
| Example 5 (5-harness weave) | Present analysis | 64.51 | 11.33 | 4.45 | 4.85 | 0.329 | 0.047 | 1.55 | 22.03 |
| | Naik (1994) | 66.33 | 11.51 | 4.93 | 4.89 | 0.342 | 0.034 | 1.46 | 21.24 |
| | Test (Foye, 1992) | 69.43 | — | — | 5.24 | — | 0.060 | — | — |

$G_{TT}$ [in fact the analytical value of $G_{TT}$ was calculated from $E_T$ and $\nu_{TT}$ as $G_{TT} = E_T/2(1 + \nu_{TT})$]. The reason may be that the Halpin-Tsai equations are essentially empirical equations designed to fit the results for $E_T$ and $G_{LT}$ well and in general they are not suitable for computing $\nu_{TT}$. Marrey and Sankar (1996) have developed an analytical method called Selective Averaging Method which compares well with the present micromechanical result for $G_{TT}$. The Selective Averaging Method yielded $G_{TT} = 3.04$ GPa for Ex. 2, which is closer to the present micromechanical result.

The results for continuum properties for all three textile composite examples (Examples 3–5) are compared with available analytical and experimental results in Table 6. Given the uncertainties and approximations in constituent material properties, description of fiber architecture, and fiber volume ratios, the results from the present method can be considered to be in good agreement with the experimental and other analytical results. It is interesting to note that the present analysis has consistently yielded slightly lower values for all elastic constants (Young's moduli and shear moduli) compared to other analytical methods. However the present method has done well in predicting the Poisson's ratios measured in tests (Foye, 1992). The Poisson's ratios agree very well with the results of Dasgupta et al. (1990). The coefficients of thermal expansion predicted by the present method are again slightly higher than those obtained using the methods of Dasgupta et al. (1990) and Naik (1994). This is due to the lower modulus values predicted by the present method.

The agreement of the method with the stiffness averaging method of Naik (1994) is only fortuitus because all the textile composite examples considered here had balanced properties in the $x$- and $y$-directions (e.g., $E_x = E_y$, $G_{xz} = G_{yz}$). If the properties in the $x$- and $y$-directions were drastically different as in the case of a simple unidirectional fiber composite, then the stiffness averaging method will predict the same $E_L$ and $E_T$, whereas rigorous micromechanics methods such as the present method will yield accurate results (see Table 5). Further, if one is interested in failure analysis of textile composites (Marrey and Sankar, 1993; Whitcomb and Srirengan, 1995), a reasonably accurate description of the stress field within the unit-cell is required and micromechanical analyses similar to the present method will have to be used.

The real thrust of this paper is to show that the plate stiffness properties of thin textile composites cannot be inferred from the continuum properties and plate thickness. The following results will demonstrate the need for computing the plate stiffness properties directly from micromechanical analysis. The equivalent $[A]$, $[B]$, $[D]$ matrices and plate CTE's were computed for the five examples. The plate properties for the bimaterial case are presented in Table 7. In this case the bimaterial plate consisted of only two layers—one layer of each material. The bimaterial plate properties were also computed using the lamination theory for two plies, and from the continuum elastic constants presented in Table 4. For example, the coefficient $D_{11}$ is obtained from the 3-D elastic constants as

$$D_{11} = \frac{E_x^M h^3}{12(1 - \nu_{xy}^{M2})}$$

*Table 7. Non-zero [A], [B] and [D] coefficients for bimaterial plate.*

| | $A_{11}, A_{22}$ $\times 10^6$ | $A_{12}$ $\times 10^6$ | $A_{66}$ $\times 10^6$ | $B_{11}, B_{22}$ $\times 10^3$ | $B_{12}$ $\times 10^3$ | $B_{66}$ $\times 10^{-3}$ | $D_{11}, D_{22}$ $\times 10^{-3}$ | $D_{12}$ $\times 10^{-3}$ | $D_{66}$ $\times 10^{-3}$ | $\alpha_x^p, \alpha_x^p$ $\times 10^{-6}$/ °C | $\beta_x^p, \beta_y^p$ /°C/m |
|---|---|---|---|---|---|---|---|---|---|---|---|
| Present analysis | 9.832 | 2.043 | 3.895 | −0.563 | −0.108 | −0.228 | 53.590 | 11.149 | 21.220 | 17.800 | 0.170 |
| Lamination theory for two plies | 9.832 | 2.043 | 3.895 | −0.563 | −0.108 | −0.228 | 53.573 | 11.131 | 21.220 | 17.814 | 0.170 |
| Lamination theory using continuum elastic constants | 9.844 | 2.048 | 3.899 | 0 | 0 | 0 | 53.762 | 11.183 | 21.293 | 8.190 | 0 |

Note: [*A*], [*B*] and [*D*] coefficients in SI units.

*Table 8. Non-zero [A], [B] and [D] coefficients for single-ply unidirectional composite.*

| | | $A_{11}$ $\times 10^6$ | $A_{12}$ $\times 10^6$ | $A_{22}$ $\times 10^6$ | $A_{66}$ $\times 10^6$ | $D_{11}$ $\times 10^{-6}$ | $D_{12}$ $\times 10^{-6}$ | $D_{22}$ $\times 10^{-6}$ | $D_{66}$ $\times 10^{-6}$ | $\alpha_x^p \times$ $10^{-6}$/°C | $\alpha_y^p \times$ $10^{-6}$/°C/m |
|---|---|---|---|---|---|---|---|---|---|---|---|
| Example 2 (uni-directional composite) | Present analysis | 0.452 | 0.062 | 0.285 | 0.114 | 2.256 | 0.224 | 0.873 | 0.568 | 7.378 | 13.188 |
| | Halpin-Tsai Eqns. and lamination theory | 0.444 | 0.039 | 0.151 | 0.045 | 3.702 | 0.328 | 1.262 | 0.371 | 6.774 | 34.239 |

Note: [*A*], [*B*] and [*D*] coefficients in SI units.

*Table 9. Non-zero [A], [B] and [D] coefficients for textile composite examples.*

| | | $A_{11}, A_{22}$ $\times 10^6$ | $A_{12}$ $\times 10^6$ | $A_{66}$ $\times 10^6$ | $B_{11}$ $\times 10^{-3}$ | $D_{11}, D_{22}$ $\times 10^{-3}$ | $D_{12}$ $\times 10^{-3}$ | $D_{66}$ $\times 10^{-3}$ | $\alpha_x^p, \alpha_y^p$ $\times 10^{-6}$/°C | $\beta_x^p$ /°C/m |
|---|---|---|---|---|---|---|---|---|---|---|
| Example 3 (Plain-weave) | Present analysis | 2.681 | 0.565 | 0.489 | 0 | 5.687 | 1.518 | 1.577 | 27.465 | 0 |
| | Mosaic model | 6.129 | 0.607 | 1.227 | 0 | 26.55 | 2.631 | 5.314 | — | — |
| | Lamination theory using continuum constants | 2.783 | 0.503 | 0.490 | 0 | 12.054 | 2.177 | 2.124 | 28.363 | 0 |
| Example 4 (Plain-weave) | Present analysis | 12.090 | 3.470 | 1.223 | 0 | 41.695 | 0.373 | 5.879 | 1.480 | 0 |
| | Mosaic model | 9.191 | 0.317 | 1.411 | 0 | 50.08 | 1.726 | 7.690 | — | — |
| | Lamination theory using continuum constants | 13.938 | 1.787 | 1.208 | 0 | 75.942 | 9.734 | 6.582 | 1.556 | 0 |
| Example 5 (5-harness weave) | Present analysis | 14.683 | 1.351 | 1.210 | 0.495* | 90.072 | 1.123 | 6.149 | 2.910 | −0.037* |
| | Lamination theory using continuum constants | 16.531 | 0.770 | 1.239 | 0 | 87.283 | 4.195 | 6.753 | 1.550 | 0 |

*In Example 5, $B_{22} = -B_{11}$ and $\beta_y^p = -\beta_x^p$.
Note: [*A*], [*B*] and [*D*] coefficients in SI units.

The finite element results for the bimaterial case were exact, i.e., identical to the results obtained with the two-ply lamination theory. The agreement in $[A]$ and $[D]$ matrices computed from the bimaterial continuum elastic constants and the two-ply lamination theory is only fortuitous because both the layers were equal in thickness. In general, however the plate properties obtained from the continuum elastic constants would be different from the two-ply lamination theory results.

The plate properties for the single-ply unidirectional composite are presented in Table 8, and for the textile composite examples in Table 9. From Tables 8 and 9 it can be seen that the plate stiffness properties and plate CTE's computed using direct micromechanics is different from those computed from continuum thermoelastic constants and plate thickness. This is especially striking in the case of $[B]$, $D_{11}$, $\{\alpha^p\}$ and $\{\beta^p\}$. It must be noted that the comparison in Table 9 is for a single layer of textile composite with one unit-cell in the thickness direction. The two results are expected to converge as the number of layers and hence the number of unit-cells in the thickness direction is increased. The actual number of unit-cells for which the continuum elastic constants can be used depends upon the inhomogeneity within the unit-cell in the thickness direction. However in many lightweight structures one can expect to use textile composites with fewer unit-cells in the thickness direction, and the present micromechanical analysis will be a useful tool. Even in thick laminated textile composites the stress distribution near the surface layers will be affected by the lack of constraints (periodic boundary conditions) on the surface, and the stress gradients obtained using the plate micromechanical analysis will shed some light on the deviation from the continuum behavior.

Ishikawa and Chou (1982, 1983a, and 1983b) have proposed computationally efficient mosaic models and other improvements of the mosaic models for predicting the plate stiffness properties of textile composites. The basic idea in these methods is that the textile composite can be modeled as a set of laminates connected in series and parallel depending on the loading direction. For the purpose of comparison the $[A,B,D]$ matrices of the plain-weave composites (Examples 3 and 4) were computed using the mosaic model, and they are presented in Table 9. It may be noted that the mosaic model highly over-predicts the plate stiffness properties. A similar observation was made by Sankar and Marrey (1993) earlier also. Some of the reasons for the over-prediction are: the actual yarn cross section in the micromechanical model is elliptical where as the mosaic model assumes a larger rectangular cross section for the yarn, and the fiber inclinations are not considered in the results presented. Even if these factors are taken into account it is expected that approximate plate models will yield a higher plate stiffness than that predicted by the rigorous micromechanical methods.

## ACKNOWLEDGEMENTS

This research was supported by the NASA Langley Research Center Grant NAG-1-1226. The authors are thankful to C. C. Poe, Jr. and Wade C. Jackson for their help and encouragement throughout the study.

## APPENDIX

In this section we will show that the stiffness matrix derived using the micromechanical analysis method described in Section 2 will always be symmetric. Without loss of generality let us consider a two-dimensional unit-cell of dimension $a \times b$ as shown in Figure 6. Let the thickness of the unit-cell in the $z$-direction be unity. Figure 6 depict the cases wherein the unit-cell is subjected to unit normal macrostrains in the $x$- and $y$-directions, respectively ($\epsilon^M_{xx} = 1$ in Figure 6(a), and $\epsilon^M_{yy} = 1$ in Figure 6(b), and all other macrostrain components are equal to zero). Let us define a system of notations to denote the forces acting

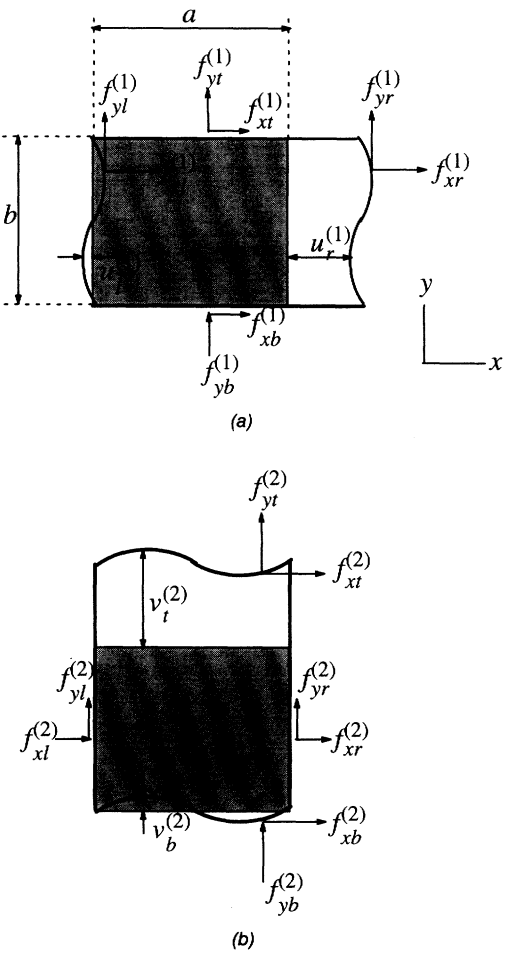


***Figure 6.*** *Notations for forces and displacements on the unit-cell boundary.*

on the sides of the unit-cell. The forces acting on the surfaces of the unit cell are denoted by $f$. Suffixes $x$ and $y$ denote forces acting in the $x$ and $y$ directions, respectively. Further the suffixes $l$ and $r$ denote the left and right surfaces of the unit-cell. Similarly suffixes $t$ and $b$ denote top and bottom surfaces of the unit-cell. Superscripts (1) and (2) are used to denote the loading cases 1 and 2 [Figure 6(a) and 6(b)] respectively. For example, $f_{yl}^{(2)}$ refers to forces acting on the left face ($x = 0$) in the $y$-direction in Figure 6(b). In the case of displacements, $u$ and $v$ refer to displacements in the $x$- and $y$-directions. For example, $v_b^{(1)}$ denotes displacement in the $y$-direction of points on the bottom surface ($y = 0$) of the unit-cell in Case 1.

Let us apply the Betti-Rayleigh reciprocal theorem (Fung, 1965) to the load cases depicted in Figure 6. Let $W_1$ be equal to the work done by the forces in Figure 6(a) through the corresponding displacements in Figure 6(b). Similarly $W_2$ represents the work done by the forces in Figure 6(b) through the corresponding displacements in Figure 6(a). Then the expressions for $W_1$ and $W_2$ can be derived as:

$$W_1 = \int_0^b (f_{xl}^{(1)} u_l^{(2)} + f_{xr}^{(1)} u_r^{(2)})dy + \int_0^b (f_{yl}^{(1)} v_l^{(2)} + f_{yr}^{(1)} v_r^{(2)})dy$$
$$\int_0^a (f_{xb}^{(1)} u_b^{(2)} + f_{xt}^{(1)} u_t^{(2)})dx + \int_0^a (f_{yb}^{(1)} v_b^{(2)} + f_{yt}^{(1)} v_t^{(2)})dx \tag{22}$$

$$W_2 = \int_0^b (f_{xl}^{(2)} u_l^{(1)} + f_{xr}^{(2)} u_r^{(1)})dy + \int_0^b (f_{yl}^{(2)} v_l^{(1)} + f_{yr}^{(2)} v_r^{(1)})dy$$
$$\int_0^a (f_{xb}^{(2)} u_b^{(1)} + f_{xt}^{(2)} u_t^{(1)})dx + \int_0^a (f_{yb}^{(2)} v_b^{(1)} + f_{yt}^{(2)} v_t^{(1)})dx \tag{23}$$

Since periodic boundary conditions are applied on the surfaces of the unit-cell, the forces on the left and right surfaces should be equal and opposite, and so are the forces on the top and bottom surfaces. For example, $f_{yl}^{(1)} = -f_{yr}^{(1)}$. The displacements of points on opposite faces of the unit-cell differ by a constant, either 0 or $a$ or $b$ depending on the loading case [see Figures 6(a) and 6(b)]. Substituting the periodic BC's in Equations (22) and (23), we find that all terms on the right hand side of Equations (22) and (23) vanish except the last term in Equation (22) and the first term in Equation (23). Then equating $W_1$ and $W_2$ we obtain

$$b \int_0^a f_{yt}^{(1)} dx = a \int_0^a f_{xr}^{(2)} dy \tag{24}$$

The above equation can be rewritten as

$$\frac{1}{a}\int_0^a f_{yt}^{(1)}\,dx = \frac{1}{b}\int_0^b f_{xr}^{(2)}\,dy \tag{25}$$

From the definition of macrostresses given by Equation (8) we obtain

$$\sigma_{yy}^{M(1)} = \sigma_{xx}^{M(2)} \tag{26}$$

Substituting the above relation in the constitutive equation of the homogenized medium (Equation 1) we obtain

$$C_{21} = C_{12} \tag{27}$$

In a similar manner all other symmetry relations ($C_{ij} = C_{ji}$) can be derived.

## REFERENCES


Agarwal, D. A. and L. J. Broutman. 1990. *Analysis and Performance of Fiber Composites,* NY: John Wiley and Sons.

Cook, R. D., D. S. Malkus and M. E. Plesha. 1989. *Concepts and Applications of Finite Element Analysis, Third Edition,* NY: John Wiley and Sons, pp. 272-274.

Dasgupta, A., S. Bhandarkar, M. Pecht and D. Barkar. 1990. "Thermo-elastic Properties of Woven-Fabric Composites Using Homogenization Techniques," *Proceedings of the American Society for Composites, Fifth Technical Conference,* Technomic Publishing Co., pp. 1001-1010.

Dexter, H. B. and J. G. Funk. 1986. "Impact Resistance and Interlaminar Fracture Toughness of Through-the-Thickness Reinforced Graphite/Epoxy," *AIAA Paper 86-1020-CP.*

Foye, R. L. 1992. "Finite Element Analysis of the Stiffness of the Fabric Reinforced Composites," *NASA CR-189597.*

Foye, R. L. 1993. "Approximating the Stress Field within the Unit-Cell of a Fabric Reinforced Composite Using Replacement Elements," *NASA CR-191422.*

Fung, Y. C. 1965. *Foundations of Solid Mechanics,* Englewood Cliffs, NJ: Prentice-Hall.

Gong, J. C. and B. V. Sankar. 1991. "Impact Properties of Three-Dimensional Braided Graphite/Epoxy Composites," *J. Comp. Materials,* 25(6):715-731.

Hart, R. 1994. "A Micromechanical Model for Predicting Thermal Conductivities in Textile Composites," *Master of Science Thesis,* Gainesville, FL: University of Florida.

Ishikawa, T. and T. W. Chou. 1982. "Elastic Behavior of Woven Hybrid Composites," *J. Comp. Mater.,* 16:2-19.

Ishikawa, T. and T. W. Chou. 1983a. "One Dimensional Micromechanical Analysis of Woven Fabric Composites," *AIAA J.,* 21:1714-1721.

Ishikawa, T. and T. W. Chou. 1983b. "In-Plane Thermal Expansion and Thermal Bending Coefficients of Fabric Composites," *J. Comp. Mater.,* 17:92-104.

Ma, C. L., J. M. Yang and T. W. Chou. 1986. "Elastic Stiffness of Three Dimensional Braided Textile Structural Composites," *Composite Materials: Testing and Design (Seventh Conference), ASTM STP 893,* pp. 404-421.

Marrey, R. V. 1995. "Finite Element Micromechanics Models for Predicting Stiffness and Strength of Textile Composite Materials," Doctoral Dissertation, Gainesville, FL: University of Florida.

Marrey, R. V. and B. V. Sankar. 1993. "Stress Gradient Effects on Stiffness and Strength of Textile

Composites," *Composite Materials and Structures,* C. W. Bert, V. Birman and D. Hui, eds., AMD-Vol. 179, New York, NY: American Society of Mechanical Engineers, pp. 133–148.

Marrey, R. V. and B. V. Sankar. 1995. "Micromechanical Models for Textile Structural Composites," *NASA CR 198229.*

Naik, R. A. 1994. "Analysis of Woven and Braided Fabric Reinforced Composites," *NASA CR-194930.*

Peters, S. T., R. F. Foral and W. D. Humphrey. 1990. "Filament Winding," S. M. Lee, (ed.) in *International Encyclopedia of Composites, Vol.,* New York, NY: VCH Publishers.

Sankar, B. V. and R. V. Marrey. 1993. "A Unit-Cell Model of Textile Composite Beams for Predicting Stiffness Properties," *Composites Science and Technology,* 49:61–69.

Sharma, S. K. and B. V. Sankar. 1995. "Effects of Through-the-Thickness Stitching on Impact and Interlaminar Fracture Properties of Textile Graphite/Epoxy Laminates," *NASA CR-195042.*

Whitcomb, J. D. 1991. "Three Dimensional Stress Analysis of Plain Weave Composites," *Composite Materials Fatigue and Fracture (Third Volume), ASTM STP 1110,* pp. 417–438.

Whitcomb, J. D. and K. Srirengan. 1995. "Effects of Various Approximations on Predicted Progressive Failure in Plain Weave Composites," *Mechanics of Textile Composites Conference, Part 2 NASA Conference Publication 3311,* October.

Whitney, T. J. and T. W. Chou. 1989. "Modeling of 3-D Angle-Interlock Textile Composite Structures," *J. Comp. Materials,* 23-29:890–911.

Yang, J. M. and T. W. Chou. 1987. "Performance Maps of Textile Structural Composites," *Sixth International Conference on Composite Materials (ICCM VI),* 5:579–588.

Yoshino, T. and T. Ohtsuka. 1982. "Inner Stress Analysis of Plane Woven Fiber Reinforced Plastic Laminates," *Bulletin of the JSME,* 25-202:485–492.